Nuclear Instruments and Methods in Physics Research A 1068 (2024) 169716

Contents lists available at ScienceDirect

Nuclear Inst. and Methods in Physics Research, A

journal homepage: www.elsevier.com/locate/nima

Full Length Article

Validation of Timepix4 energy calibration procedures with synchrotron X-ray beams

P. Delogu [a,b], N.V. Biesuz [c,d], R. Bolzonella [c,d], L. Brombal [e,f], V. Cavallini [c,d], F. Brun [g,f], P. Cardarelli [c,d], A. Feruglio [h,b,*], M. Fiorini [c,d], R. Longo [e,f], V. Rosso [h,b]

[a] Dipartimento di Scienze Fisiche, della Terra e dell'Ambiente, Università di Siena, Via Roma 56, Siena, 53100, Italy
[b] INFN Pisa, Largo Bruno Pontecorvo 3, Pisa, 56127, Italy
[c] Dipartimento di Fisica e Scienze della Terra, Università degli Studi di Ferrara, Via Saragat 1, Ferrara, 44122, Italy
[d] INFN Ferrara, Via Saragat 1, Ferrara, 44122, Italy
[e] Dipartimento di Fisica, Università degli Studi di Trieste, Via Valerio 2, Trieste, 34127, Italy
[f] INFN Trieste, Via Valerio 2, Trieste, 34127, Italy
[g] Dipartimento di Ingegneria e Architettura, Università degli Studi di Trieste, Via Valerio 10, Trieste, 34127, Italy
[h] Dipartimento di Fisica, Università di Pisa, Largo Bruno Pontecorvo 3, Pisa, 56127, Italy

ARTICLE INFO

Keywords:
X-rays
Hybrid detectors
Pixel detectors
Energy calibration
Timepix4
Spectroscopic performances

ABSTRACT

The Timepix4 is an application-specific integrated circuit developed by the Medipix4 collaboration. The chip is a 448 × 512 matrix that can be connected, via bump-bonding, to pixelated sensors of various materials and thicknesses, forming application specific detection systems. Among the Timepix4 operating modes, the data-driven Time-of-Arrival - Time-Over-Threshold is a particularly promising mode for spectral imaging applications: data packets are generated every time the charge created by the incoming radiation goes above a pre-defined threshold, allowing the count of the detected particles and their energy measurement. This article investigates the spectroscopic characteristics of a Timepix4 assembly equipped with a 300 μm Si sensor, using monochromatic X-ray beams in the energy range 8.5 keV–40 keV working at the SYRMEP beamline of the Elettra synchrotron. The accuracy and the energy resolution of the reconstructed energy spectra, together with an energy resolution model, will be presented.

1. Introduction

Timepix4 [1] is the last generation application-specific integrated circuit (ASIC) of the Timepix family, developed by the Medipix4 collaboration [2]. The Timepix4 hybrid detection system comprises a 448 × 512 readout system connected via bump-bonding to semiconductor sensors with a square pixel layout (55 μm pitch). Various sensor materials and thicknesses can be used to optimize the detector performances in several applications.

Each pixel of the ASIC comprises an analog front-end [3,4] and a digital part [1]. In the former there are, a charge-sensitive amplifier and a discriminator that compare the pre-amplified output with a threshold value. The analog front-end can be configured in various gain modes to cope different applications acting on a feedback capacitance; additionally, the shape of the analogic pulse is influenced by the Krummenacher current (Ikrum), which determines the return-to-zero time of the signal and the system dead time. The threshold of the discriminator can be adjusted at the pixel level via a local DAC, allowing the equalization of the thresholds for all the pixels. When the discriminator output is above the fixed threshold, the signal is digitized, and information is stored in registers. Different operating modes are available: frame-based photon counting, data-driven photon counting and Time over Threshold (ToT) - Time of Arrival (ToA) data-driven. In the ToT-ToA data-driven mode, output packets are generated every time a pixel is hit, providing information on the events' ToA, acquired with a time bin of 195 ps, and on the signal's ToT. After calibrating the detection system, ToT can be used to measure the energy deposition of the incident radiation in each pixel.

When radiation interacts with the sensor, energy is released, and an electron–holes charge cloud is created in the semiconductor and driven to the collection electrodes by an electric field. During the collection process the charge cloud diffuse and, depending on its position, can be shared among multiple pixels forming a cluster. By combining the ToA and ToT information, it is possible to perform the clusterisation of the hits reconstruct the individual events, and measure the deposited

* Corresponding author at: Dipartimento di Fisica, Università di Pisa, Largo Bruno Pontecorvo 3, Pisa, 56127, Italy.
E-mail address: a.feruglio@studenti.unipi.it (A. Feruglio).

https://doi.org/10.1016/j.nima.2024.169716
Received 7 May 2024; Received in revised form 18 July 2024; Accepted 7 August 2024
Available online 18 August 2024

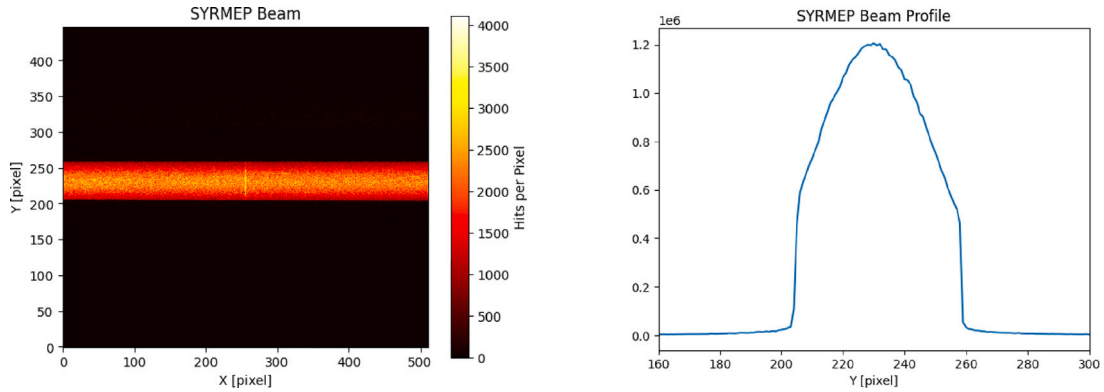

Fig. 1. Left: beam cross section on the detector (38 keV acquisition); the beam covers more than the entire length of the detector along the X-axis (28.2 mm), while along the Y-axis, the vertical direction of the set-up, the beam extension is 3 mm. Right: Gaussian-like profile, defined by the tungsten slits, of the beam along the Y-axis: the profile extends over 54 pixels.

energy. The size of clusters depends on the incident radiation, on the released energy and on applied threshold.

In data-driven mode, information on the single hit is encoded in 64-bit data packets. The matrix readout is performed via up to 16 fast links, each with a bandwidth of 10 Gb/s. Timepix4 is therefore capable to process correctly up to approximately 3.6 $\cdot 10^6$ hits mm^{-2} s^{-1}. The detector's ability to acquire data with a continuous energy spectrum, even in high-rate conditions, makes it a very promising tool for spectral imaging [5], and a systematic investigation of the Timepix4 spectral capabilities is essential to understand its potential in X-ray imaging applications.

In this work, we present the results of the analysis performed on a dataset acquired using a tunable, monochromatic, synchrotron beam as a radiation source to validate two different calibration procedures and measure the energy resolution of a Timepix4 detection system with respect to X-ray energy.

2. Materials and methods

2.1. Monochromatic photon beam

The acquisitions were performed at the SYRMEP (SYnchrotron Radiation for Medical Physics) beamline of the Elettra Synchrotron in Trieste [6]. The synchrotron radiation is monochromatized with two Si (111) crystals in Bragg diffraction geometry; by acting on the angle of the two Si crystals system with respect to the incoming synchrotron beam, it is possible to select the energy of the photons in a range between 8.5 keV and 40 keV, with an uncertainty of energy monochromacity $\Delta E/E \simeq 2 \cdot 10^{-3}$. The beam's intensity, monitored through an ionization chamber, can be tuned either through the use of aluminum filters or by de-tuning the second crystal of the monochromator. The beam cross-section on the detector, shown in Fig. 1 (left), was defined by tungsten slits. The beam width, 28.6 mm, is larger than the detector extent, while in the vertical direction the beam is 3 mm high. The vertical profile of the beam, shown in Fig. 1 (right), is Gaussian-like.

Eighteen X-rays energy values were selected in the available energy range: nine energy values were used to calibrate the detection system, and the remaining energy values to measure the spectroscopic performances of the detection system.

2.2. Measurement set-up

The used Timepix4_v2 detection system was equipped with a 300 μm thick Si p-on-n sensor produced by Advafab Oy [7] and reversed biased at 100 V. To control the detection system, the Timepix4 was connected to the SPIDR4 readout system produced by Nikhef [8], which, in turn, is connected to the data acquisition PC exploiting the 1 Gbps Ethernet connection for the device configuration and using 2 of the 16 fast links, each operating at 2.56 Gbps, for data readout. An in-house software allows to configure the system, acquire data and monitor the acquisitions.

The measurements were performed in ToT-ToA data-driven mode. The pre-amplifier was set in high-gain mode (feedback capacitance = 3fF), the Ikrum was set at 1.96 nA. The threshold was fixed at 1000 e^- (3.62 keV) and uniformed all over the matrix applying the equalization procedure with a dedicated software.

To keep the Timepix4 temperature stable during the acquisitions, a chiller was connected to the chipboard with a custom-made cooling system. The chiller was operated at 15 °C, and the temperature of the sensor was monitored during the acquisitions and it was in the range 16 °–17 °C. The whole detection system was placed on a motorized hexapod to control its position and its motion. An image of the measurement set-up is shown in Fig. 2.

2.3. X-ray calibration

A specific procedure was developed to compute, pixel by pixel, the conversion parameters necessary to determine the energy deposited by the detected photons from the measurement of the ToT of the signal. A series of flat fields images were acquired for nine energy values: 8.5 keV, 10 keV, 12 keV, 16 keV, 20 keV, 24 keV, 28 keV, 32 keV, 38 keV. Each flat field was obtained through a scan, in which the Timepix4 detection system was moved vertically at a constant speed (2 mm/s) to obtain a uniform irradiation of the surface with the laminar beam. For each energy, an high number of events was acquired (4000 hits per pixel) to reduce the statistical variability. To limit the size of each acquired file, the beam's intensity was adjusted to obtain approximately 100 hits per pixel in each scan and 40 scans were repeated at each energy.

2.3.1. Data analysis

The acquired data were initially clustered using the information on the ToA and the location of the hits. Since the calibration has to be performed pixel by pixel, only the photon whose charge was fully collected in a single pixel has to be considered: these corresponds to events with cluster size equal to one.

The calibration procedure foresees several steps that are done in succession. For each sampled energy, the measured ToT distributions was plotted, and the average ToT of the spectrum ($\overline{ToT}$) was calculated using a Gaussian fit. Since the ToT distributions resulted asymmetric with a long tail toward energies lower than the photopeak value, the Gaussian fits were performed considering only a limited region of the ToT photopeak excluding, in this way, the events not fully collected.

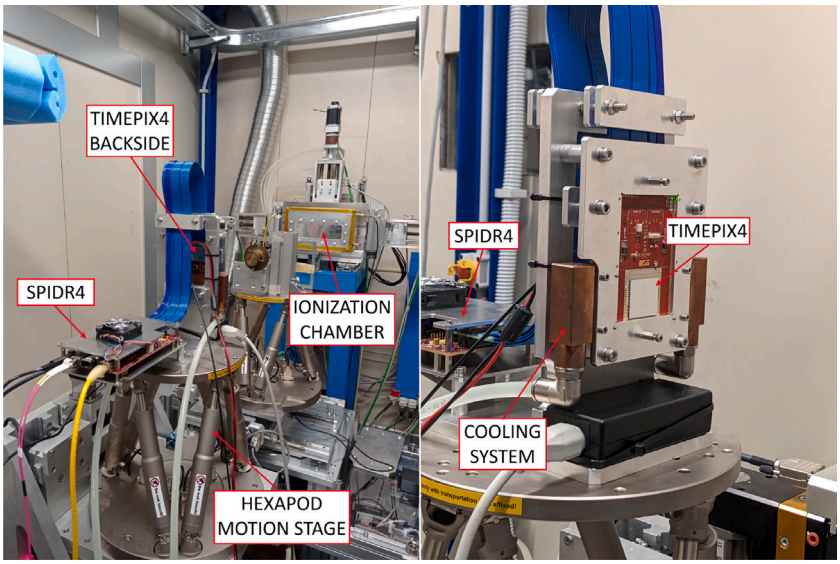

Fig. 2. Left: global view of the measurement set-up: the SPIDR4 readout periphery and the Timepix4 chipboard, connected via blue flat cables, are placed on the hexapod motion stage; the ionization chamber is located between the beam exit window and the Timepix4 detector; right: a zoom on the detection system seen from the front (beam eye view); the Si sensor and the cooling system are visible.

The $\overline{ToT}$ obtained for all the sampled energies were plotted as a function of energy, and a fit of the four parameters Timepix4 calibration function [9] was performed:

$$\overline{ToT} = a \cdot E + b - \frac{c}{E - t}. \tag{1}$$

This procedure was repeated for each pixel of the detecting system.

2.4. Mixed calibration with test-pulses and X-ray

Since the Timepix4 calibration curve is non-linear in the low energy region and taking into account that the lowest beam energy available at SYRMEP is 8.5 keV, the calibration procedure would benefit from an extension of the calibration range.

Timepix4 allows the injection of controlled quantities of charge into the pixels of the ASIC by sending voltage pulses to capacitors located in the analog front-end of each pixel, allowing a preliminary device calibration. However, due to the uncertainty associated with the nominal value of the capacitances, a calibration based only on test-pulses induces an error in the energy reconstruction of the detected photons and a sub-optimal energy resolution. A correction to the data acquired via test-pulses must be implemented to use them to calibrate the Timepix4; this correction can be made by combining test-pulses acquisitions with data acquired with an X-ray source [10].

The test-pulses acquisitions were made under the same measurement settings as the X-ray acquisitions. 500 events were acquired at each energy value for each pixel, sampling 17 points in a nominal energy range between 4.7 keV and 50.7 keV.

2.4.1. Data analysis

The data acquired via test-pulses were analyzed by repeating the same procedure presented in Section 2.3.1 to get for each pixel the ToT vs Energy plot.

The correction procedure begins with the analysis of the linear part of these plot, considering only the points with a nominal energy higher than a fixed value. For each pixel, a linear fit was initially performed on the data acquired with the X-ray source to determine the two parameters a_{lin} and b_{lin}:

$$ToT_{XRays} = a_{lin} \cdot E_{XRays} + b_{lin}. \tag{2}$$

A second fit was then performed on the data acquired via test-pulses:

$$ToT_{TP} = a_{lin} \cdot E_{TP} \cdot g + b_{lin} + h. \tag{3}$$

a_{lin} and b_{lin} are the parameters fixed by the previous fit, while g and h are the two free parameters that correct respectively E_{TP} and ToT_{TP}. With the described procedure, the values of g and h were determined all over the pixels, providing to two 448 × 512 matrices. After the correction procedure, the points acquired via test-pulses and those acquired with the X-ray source describe the same calibration curve in a ToT vs Energy plot. The four matrices with the calibration parameters a_{mixed}, b_{mixed}, c_{mixed}, and t_{mixed} were determined by fitting X-rays and test-pulses corrected data with Eq. (1).

2.5. Energy spectra reconstruction

The conversion parameters obtained with the different calibration procedures were used to reconstruct the energy spectrum of the photons acquired in flat-field scans at nine energies: 9 keV, 11 keV, 14 keV, 18 keV, 22 keV, 26 keV, 30 keV, 34 keV and 40 keV.

While in the calibration procedure only the events detected within a single pixel were used, in the spectra reconstruction also cluster size two and three events were considered. Since the pixel threshold is fixed, we expect a higher percentage of events with cluster size > 1 in higher energies acquisitions.

The photopeaks positions (μ) and their widths (σ) were measured by performing a Gaussian fit on the spectra. The accuracy of the nine reconstructed X-ray photopeaks was evaluated by calculating the relative error defined as: $|E - \mu|/E$.

The detector's energy resolution, defined as FWHM/E, was calculated for each energy, and the calculated energy resolutions were fitted with the Gaussian energy broadening function [11,12]:

$$\frac{FWHM}{E} = \frac{p_1 + p_2 \cdot \sqrt{E + p_3 \cdot E^2}}{E} \tag{4}$$

The parameters p_1, p_2 and p_3 can be used to provide a model of the detector response for Monte Carlo simulations [13].

3. Results

3.1. X-ray calibration

As already told, the energy calibration in Timepix4 detection system is fundamental both to convert ToT measurements into energy and to reduce the spread of the pixels responses.

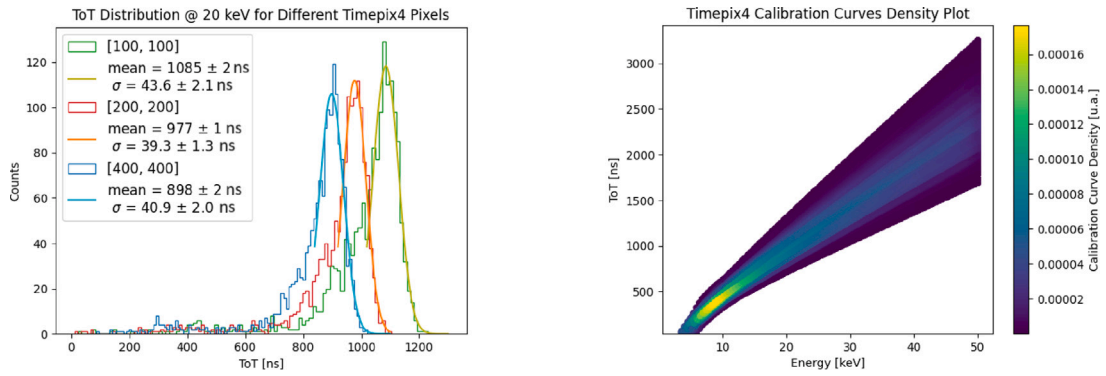

Fig. 3. Left: ToT distribution measured by three pixels at 20 keV (pixel coordinates are reported in the legend); the Gaussian fit on each ToT distribution is also reported (results in the legend), highlighting the asymmetric interval. Right: density plot of the calibration curves for all the Timepix4 pixels.

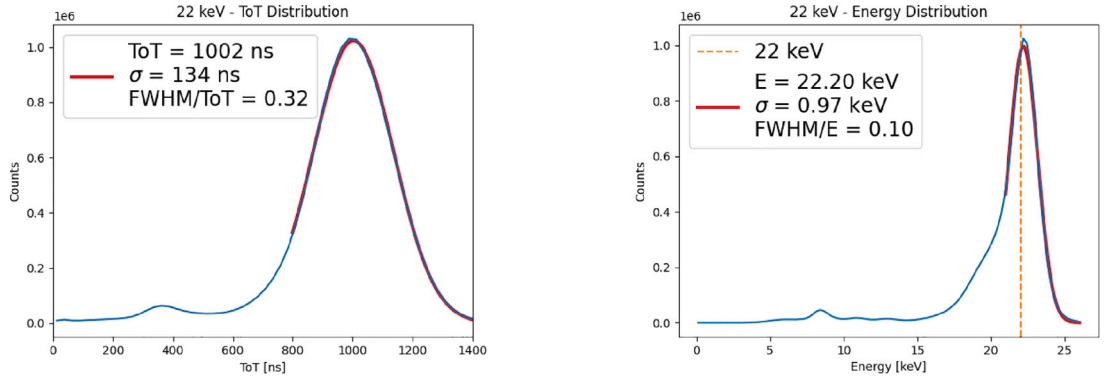

Fig. 4. Left: 22 keV photons ToT spectra (full-matrix acquisition, all cluster size). Right: 22 keV photons energy spectra (full-matrix acquisition, all cluster size); the dashed line represents the energy of the photons. The Gaussian fits are superimposed on the data on both plots.

The first step to obtain the calibration curves is to construct the ToT distribution for each energy and for each pixel, considering only events with cluster size one. Fig. 3 (left) shows some ToT spectra measured by different Timepix4 pixels in a 20 keV photons acquisition. A Gaussian fit is then performed on each distribution providing the average $\overline{ToT}$. The fits were performed partially excluding the left sides of the photo-peaks, as shown in Fig. 3 (left), to be sure to consider only fully-collected-charge events.

The procedure was repeated on all energy acquisitions, providing for each pixel a $\overline{ToT}$ vs Energy plot.

Finally, by fitting Eq. (1) on these data, the ToT to Energy conversion parameters a, b, c and t are calculated for each pixel.

Fig. 3 (right) shows a density plot of the calibration curves obtained on all the pixel matrix: the spread of the plot shows the differences in pixel response to the same signal.

3.1.1. Energy distribution reconstruction after X-ray calibration

To verify the calibration results, the conversion parameters were used to convert the ToT spectra, measured in full matrix acquisitions, into energy spectra, considering all cluster size events.

In Fig. 4 is reported, as an example, a comparison between the ToT distribution (left) and the energy distribution (right) acquired at 22 keV.

The calibration compensates for the different response of the pixels reducing the width of the spectra: $\Delta ToT/ToT = 32\%$, while $\Delta E/E = 10\%$.

The energy spectrum of the photo-peak results asymmetric due to charge-lost effect: when the deposited charge is below the threshold, a small fraction of the energy is lost and the total measured energy will be lower than the nominal photon value.

The photopeaks $\mu_{x-ray\ cal}$ and $\sigma_{x-ray\ cal}$ were determined by performing Gaussian fits on the single peaks. Table 1 resumes the results obtained for the nine energies. The errors on $\mu_{x-ray\ cal}$ and $\sigma_{x-ray\ cal}$, evaluated by the fit, are less than 0.01 keV over the all energy range. The accuracy of each energy is also reported in Table 1 and results less than 1.5%.

Table 1
Photopeaks $\mu_{x-ray\ cal}$ and $\sigma_{x-ray\ cal}$ obtained with the X-ray calibration parameters all over the matrix.

Nominal X-ray energy [keV]	$\mu_{x-ray\ cal}$ [keV]	$\sigma_{x-rays\ cal}$ [keV]	$\lvert E - \mu_{x-ray\ cal}\rvert/E$
9	9.04	0.65	0.4%
11	11.12	0.81	1.1%
14	14.21	0.89	1.5%
18	18.23	0.92	1.3%
22	22.20	0.97	0.9%
26	26.26	1.02	1.0%
30	30.25	1.08	0.8%
34	34.21	1.09	0.6%
40	40.30	1.18	0.7%

The energy resolutions are comparable to the results previously obtained, in the same operating mode, with a Timepix3 ASIC equipped with a 300 μm thick Si sensor [11].

3.2. Mixed calibration with test-pulses and X-ray

To extend the calibration energy range, test-pulses acquisition were performed. Fig. 5 (left) shows, for the same pixel, the comparison between the calibration curves obtained using the X-ray acquisitions and the test pulses acquisitions. As expected, the two curves differ, and the points acquired via test-pulses need to be corrected according to the method reported in Section 2.4.1.

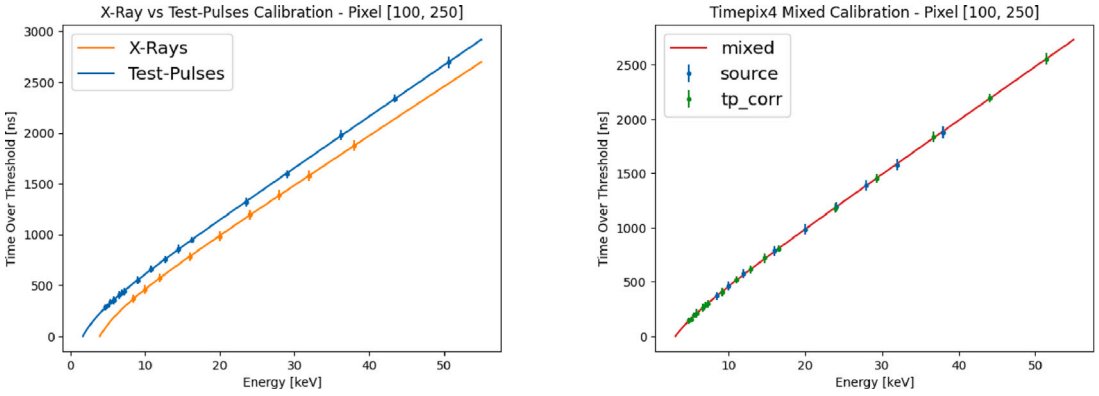

Fig. 5. Left: comparison between the calibration curves obtained using the X-ray acquisitions and the test-pulses acquisitions. Right: fit of the calibration curves on both the X-ray points and test-pulses corrected points. The two plot refers to the same pixel [100, 250].

Table 2
Photopeaks μ_{mixed} and σ_{mixed} obtained with the mixed calibration parameters evaluated all over the matrix.

Nominal X-ray energy [keV]	μ_{mixed} [keV]	σ_{mixed} [keV]	$\lvert E - \mu_{mixed}\rvert/E$
9	8.99	0.62	0.1%
11	11.09	0.67	0.8%
14	14.18	0.71	1.2%
18	18.20	0.78	1.1%
22	22.17	0.85	0.8%
26	26.18	0.91	0.7%
30	30.15	0.95	0.5%
34	34.17	0.99	0.5%
40	40.05	1.08	0.1%

Fig. 5 (right) shows that, after the correction procedure, all the points belong to the same calibration curve; the conversion parameters are obtained by fitting the data with Eq. (1).

3.2.1. Energy distribution reconstruction after mixed calibration

The new conversion parameters obtained with the mixed calibration procedure, were used to convert ToT spectra into energy spectra for the selected nine energy values. The μ_{mixed} and σ_{mixed} of the energy spectra were obtained with the procedure seen in Section 3.1.1 and are reported in Table 2.

The mixed calibration procedure reduces both the σ values and the shift of the photopeak position: the accuracy results less than 1.2%.

3.3. Different cluster-size events energy distributions

In the previous paragraphs the energy resolution was calculated considering all events regardless of the cluster size. The population of the three clusters sizes varies; at low energies, clusters with size 1 are the majority, while increasing the energies clusters with sizes 1 and 2 became almost equally populated; finally, events with cluster size 3 appears only at higher energies and represents less then the 5% of the total, as shown in Fig. 6.

Some of energy spectra acquired at different energies are reported in Fig. 7. In each plot, the energy distributions of clusters of sizes 1, 2, and 3 are represented separately. In particular, the left column show the results obtained at 9 keV, 22 keV and 40 keV with the X-rays calibration, while the right columns shows the ones obtained with the mixed calibration. The position (μ) of the photopeaks are reported in the legends.

For single pixel events, the accuracy of the photopeaks position is less than 1%. As expected, no significant differences are observed if we compare the results obtained after the X-rays calibration and after the mixed calibration: the energy of the analyzed events is located in the linear region of the calibration curve, which we expect to remain almost the same between the two procedures.

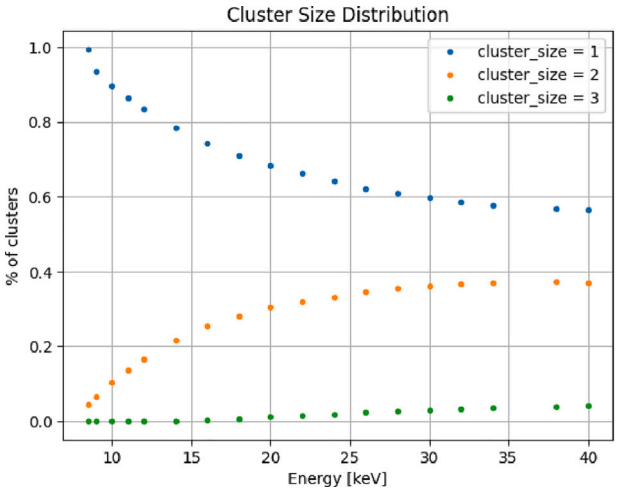

Fig. 6. Percentage of clusters with size 1, 2 and 3 as a function of energy.

Looking at the distribution of cluster size two events obtained after the X-rays calibration, a shift with respect to the photons nominal energies is observed. This shift, particularly evident at low energies, is strongly reduced in the results obtained after applying the mixed calibration procedure (the accuracy at 9 keV goes from 20.6% to 2.4%).

Finally, for three pixels events, as expected, the shift of the calculated photopeaks position with respect to the photon nominal values is greater in comparison with the shift of cluster size one and two events, as the total charge results from the sums of three signal, of which some values can be very small.

The same photopeaks asymmetries observed in Fig. 4 and related to charge-sharing are visible in the spectra. This effect is particularly evident for low energies X-rays, where it is more likely that a part of the charge shared between multiple pixels falls below the fixed energy threshold and is lost. At higher X-rays energies the asymmetry is strongly reduced.

Looking at the 22 keV and 40 keV energy spectra reported in Fig. 7, several peaks in addition to the full energy peaks appears: some of these energies are compatible within 2%, with some elements present in detection system, in particular copper (8.04 keV) and tin (25.27 keV).

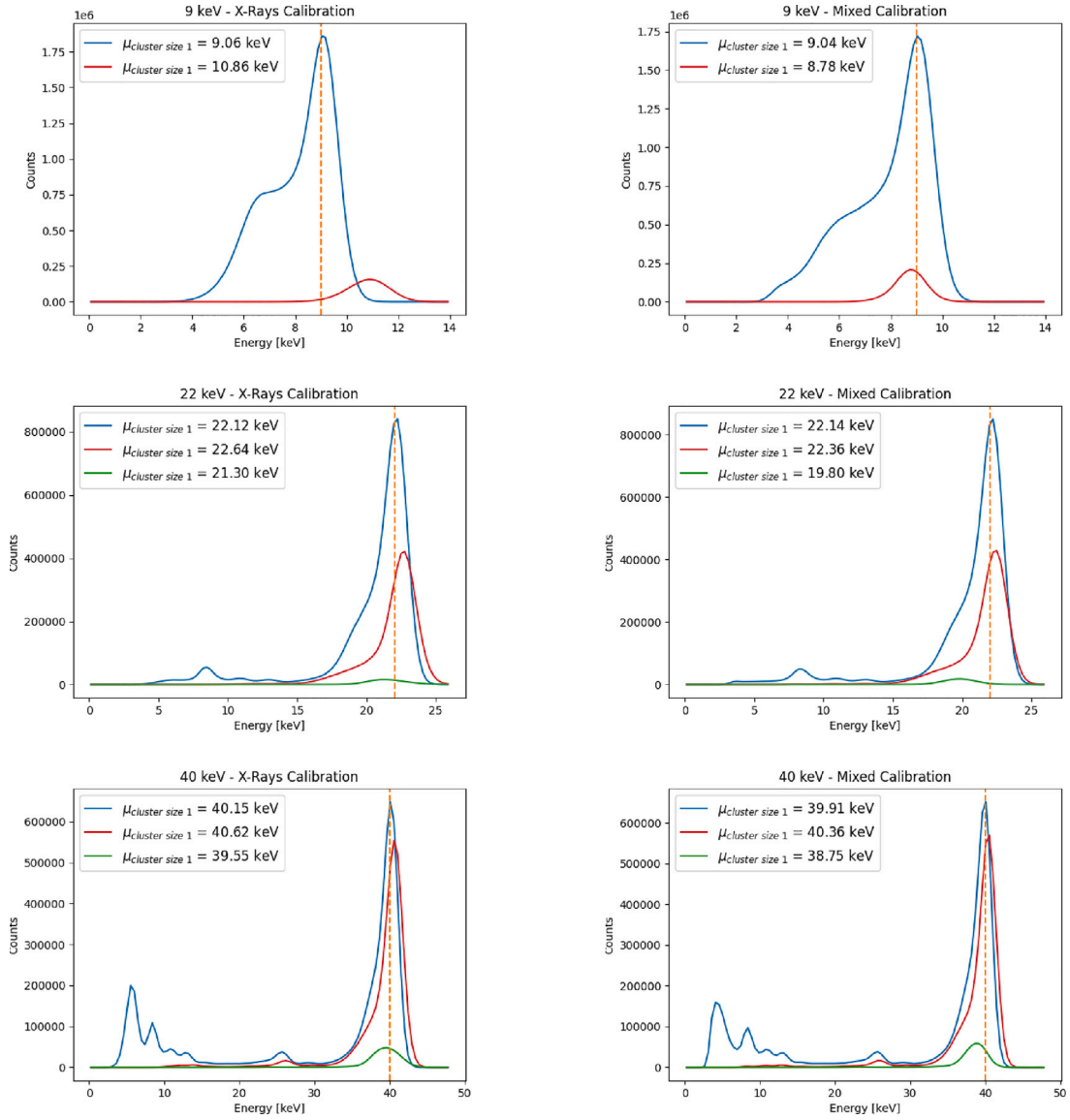

Fig. 7. Energy spectra reconstructed at selected energies: 9 keV, 22 keV and 40 keV. Events with cluster size one, two and three are plotted separately; the dashed lines represent photon energies; the photopeaks positions are reported in the legends. Left column: results obtained after the X-rays calibration; Right column: results obtained after the mixed calibration.

3.4. Energy resolution

The Timepix4 energy resolution behavior as a function of the energy obtained after the X-ray calibration procedure and the mixed calibration procedure was studied and reported in Fig. 8.

The mixed calibration procedure produce a better energy resolution than the X-ray calibration. The improvements, more evident at low energies, are related to the better energy reconstruction of two-pixels cluster, as discussed in Section 3.3.

To have a model of the energy resolution behavior, the mixed calibration point were fitted with the Gaussian energy broadening function (Eq. (4)) and it is also reported in Fig. 8.

The obtained energy resolutions are slightly better with respect to previous result [11,14].

4. Conclusion

The spectroscopic characterization of a hybrid detection system, based on Timepix4 ASIC and a Si pixelated detector, was performed. The calibration of the detection system plays a fundamental role and was performed using experimental data collected at the SYRMEP beamline of the Elettra synchrotron. Different calibration procedures were performed, and the best spectral performance was obtained using a mixed calibration procedure that combines data acquired through test-pulses internally generated by the ASIC and synchrotron X-ray beams. Several X-ray beams in the energy range 9 keV–40 keV were used to determine the energy resolution and the accuracy capabilities of the detection system. The accuracy in energy is better than 1,2% while the energy resolution at 40 keV turned out to be 6,4%. The calculated energy resolution function indicates that for X-ray beams above 20 keV the relative energy resolution of the system will be better than 10%.

The spectroscopic performances of the studied detection system demonstrate its suitability to be applied in K-edge imaging and simultaneous imaging of multiple contrast agents: studies in these field are planned.

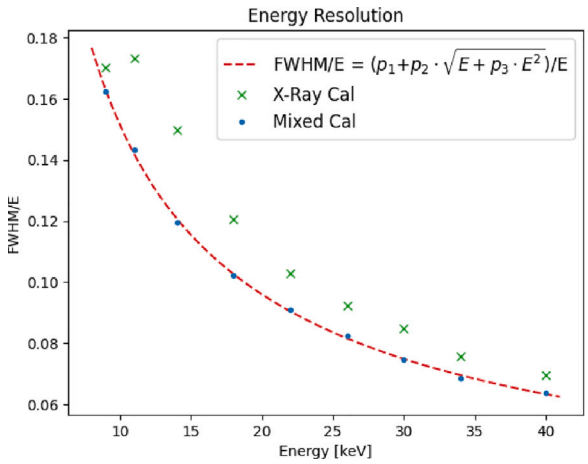

Fig. 8. Timepix4 energy resolution obtained with the X-ray calibration procedure (green) and with the mixed calibration procedure (blue). The Gaussian broadening energy function is superimposed to the mixed calibration data. The obtained fit parameters and the χ^2 are: p_1 = 0.59 keV, p_2 = 0.29 keV$^{1/2}$, p_3 = 3.15 $\cdot 10^{-3}$ keV^{-1}, $\chi^2_{reduced}$ = 0.63, $\chi^2_{reduced}$ = 0.79.

CRediT authorship contribution statement

P. Delogu: Writing – review & editing, Writing – original draft, Methodology, Data curation, Conceptualization. **N.V. Biesuz:** Writing – review & editing, Software, Data curation. **R. Bolzonella:** Writing – review & editing, Software, Data curation. **L. Brombal:** Writing – review & editing, Data curation. **V. Cavallini:** Writing – review & editing, Software, Data curation. **F. Brun:** Writing – review & editing, Data curation. **P. Cardarelli:** Writing – review & editing, Data curation. **A. Feruglio:** Writing – original draft, Data curation. **M. Fiorini:** Writing – review & editing, Supervision. **R. Longo:** Writing – review & editing, Supervision. **V. Rosso:** Writing – review & editing, Supervision.

Declaration of competing interest

The authors declare that they have no known competing financial interests or personal relationships that could have appeared to influence the work reported in this paper.

Data availability

Data will be made available on request.

Acknowledgments

This work was carried out in the context of the Medipix4 Collaboration based at CERN, and partially supported by the MEDIPIX4 project funded by the INFN (National Institute for Nuclear Physics), CSN5 (National Scientific Commission 5).

We acknowledge Elettra Sincrotrone Trieste for providing access to its synchrotron radiation facilities and for financial support under the IUS internal project.

References

[1] X. Llopart Cudie, J. Alozy, R. Ballabriga, M. Campbell, R. Casanova, V. Gromov, E.H. Heijne, T. Poikela, E. Santin, V. Sriskaran, L. Tlustos, A. Vitkovskiy, Timepix4, a large area pixel detector readout chip which can be tiled on 4 sides providing sub-200 ps timestamp binning, J. Instrum. 17 (2022) http://dx.doi.org/10.1088/1748-0221/17/01/C01044.

[2] Medipix4, 2024, [Online]. https://medipix.web.cern.ch/medipix4. (Accessed 26 March 2024).

[3] R. Ballabriga, J.A. Alozy, F.N. Bandi, G. Blaj, M. Campbell, P. Christodoulou, V. Coco, A. Dorda, S. Emiliani, K. Heijhoff, E. Heijne, T. Hofmann, J. Kaplon, A. Koukab, I. Kremastiotis, X. Llopart Cudie, M. Noy, A. Paterno, M. Piller, J.M. Sallesse, V. Sriskaran, L. Tlustos, M. van Beuzekom, The Timepix4 analog front-end design: Lessons learnt on fundamental limits to noise and time resolution in highly segmented hybrid pixel detectors, Nucl. Instrum. Methods Phys. Res. A 1045 (2023) http://dx.doi.org/10.1016/j.nima.2022.167489.

[4] K. Heijhoff, K. Akiba, R. Ballabriga, M.V. Beuzekom, M. Campbell, A.P. Colijn, M. Fransen, R. Geertsema, V. Gromov, X. LlopartCudie, Timing performance of the Timepix4 front-end, J. Instrum. 17 (2022) http://dx.doi.org/10.1088/1748-0221/17/07/P07006.

[5] A. So, S. Nicolaou, Spectral computed tomography: Fundamental principles and recent developments, Korean J. Radiol. 22 (2021) http://dx.doi.org/10.3348/kjr.2020.0144.

[6] G. Tromba, R. Longo, A. Abrami, F. Arfelli, A. Astolfo, P. Bregant, F. Brun, K. Casarin, V. Chenda, D. Dreossi, M. Hola, J. Kaiser, L. Mancini, R.H. Menk, E. Quai, E. Quaia, L. Rigon, T. Rokvic, N. Sodini, D. Sanabor, E. Schultke, M. Tonutti, A. Vascotto, F. Zanconati, M. Cova, E. Castelli, The SYRMEP beamline of elettra: Clinical mammography and bio-medical applications, AIP Conf. Proc. 1266 (2010) http://dx.doi.org/10.1063/1.3478190.

[7] Advafab, 2022, [Online]. https://advafab.com/. (Accessed 22 April 2024).

[8] Home, 2018, [Online]. https://www.nikhef.nl/en/. (Accessed 19 April 2024).

[9] J. Jakubek, J. Dammer, T. Holy, M. Jakubek, S. Pospisil, V. Tichy, J. Uher, D. Vavrik, Spectrometric properties of TimePix pixel detector for x-ray color and phase sensitive radiography, in: IEEE Nuclear Science Symposium Conference Record, Vol. 3, 2007, http://dx.doi.org/10.1109/NSSMIC.2007.4436610.

[10] D. Turecek, J. Jakubek, M. Kroupa, P. Soukup, Energy calibration of pixel detector working in time-over-threshold mode using test pulses, in: IEEE Nuclear Science Symposium Conference Record, 2011, http://dx.doi.org/10.1109/NSSMIC.2011.6154668.

[11] G. Amoyal, Y. Menesguen, V. Schoepff, F. Carrel, M. Michel, J.C. Angelique, N.B.D. Lanaute, Evaluation of Timepix3 Si and CdTe hybrid-pixel detectors' spectrometric performances on X- And Gamma-rays, IEEE Trans. Nucl. Sci. 68 (2021) http://dx.doi.org/10.1109/TNS.2020.3041831.

[12] E.E. Zadeh, S.A.H. Feghhi, E. Bayat, G.H. Roshani, Gaussian energy broadening function of an HPGe detector in the range of 40 keV to 1.46 MeV, J. Exp. Phys. 2014 (2014) http://dx.doi.org/10.1155/2014/623683.

[13] L. Brombal, L. Rigon, F. Arfelli, R.H. Menk, F. Brun, A Geant4 tool for edge-illumination X-ray phase-contrast imaging, J. Instrum. 17 (2022) http://dx.doi.org/10.1088/1748-0221/17/01/C01043.

[14] J. Jakubek, Precise energy calibration of pixel detector working in time-over-threshold mode, Nucl. Instrum. Methods Phys. Res. A 633 (2011) http://dx.doi.org/10.1016/j.nima.2010.06.183.